Biomacromolecules

pubs.acs.org/Biomac

Article

Quantitatively Fine-Tuning the Physicochemical and Biological Properties of Peptidic Polymers through Monodisperse PEGylation

Xuemeng Wang, Yu Li, Tingjuan Wu, Zhigang Yang, Xing Zheng, Shizhen Chen, Xin Zhou,* and Zhong-Xing Jiang*

Cite This: *Biomacromolecules* 2020, 21, 725−731

Read Online

ACCESS | Metrics & More | Article Recommendations | Supporting Information

ABSTRACT: In biomedicine, PEGylation is one of the most successful strategies to modify the physicochemical and biological properties of peptides, proteins, and other biomacromolecules. Because of the polydisperse nature of regular PEGs and limited PEGylation strategies, it is challenging to quantitatively fine-tune and accurately predict the properties of biomacromolecules after PEGylation. However, such fine-tuning and prediction may be crucial for their biomedical applications. Herein, some monodisperse PEGylation strategies, including backbone PEGylation, side-chain PEGylation, and highly branched PEGylation, have been developed. In a comparative fashion, the impact of PEGylation strategies and monodisperse PEG sizes on the physicochemical and biological properties, including lipophilicity, thermosensitivity, biocompatibility, plasma stability, and drug delivery capability, of peptidic polymers has been quantitatively studied. It was found that the physicochemical and biological properties of PEGylated peptidic polymers can be quantitatively fine-tuned and accurately predicted through these monodisperse PEGylation strategies. After the comparative study, a side-chain monodisperse PEGylated peptidic polymer was chosen as fluorine-19 magnetic resonance and fluorescence dual-imaging traceable drug delivery vehicle. Our study may not only promote the transformation of PEGylation from an empirical technology to a quantitative science but also shed light on the rational design of PEGylated biomaterials and pharmaceutics.

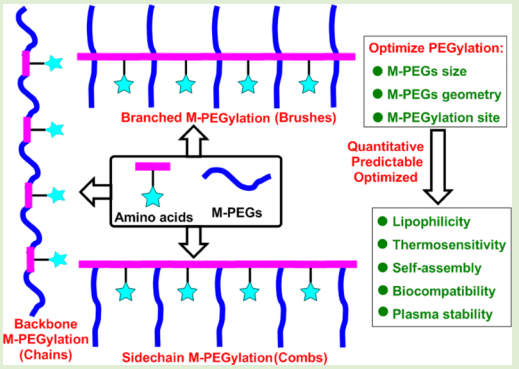

INTRODUCTION

As a class of versatile polymers with high biocompatibility and the so-called "stealth" effects, polyethylene glycols (PEGs) are the most used "gold standard" polymers in biomedicine,[1−5] which have been extensively used in pharmaceutical R&D to improve solubility and stability, reduce immunogenicity and dosing frequency, and prolong the blood circulation time.[6−9] Although it is a widely used strategy with 17 PEGylated drugs on the market (data from www.fda.gov), PEGylation is still an empirical technology rather than a quantitative science. First, as heterogeneous polymers of ethylene oxide, regular PEGs are polydisperse homologous mixtures with a wide range of molecular weights.[10−13] Even though the polydispersity of regular PEGs is obvious, they are still overwhelmingly used in biomedicine.[6−9] Moreover, the heterogeneity in PEGylated products is further amplified by PEGylation reactions because of multiple PEGylation sites, side reactions, and incomplete reactions, which leads to difficulties in the chemical processes (i.e., monitoring PEGylation reaction, product purification, and characterization), uncertainty in downstream applications, low reproducibility of related studies, and so forth.[14−17] Second, the choice of PEGs and PEGylation sites is usually empirical, which is mainly determined by the availabilities of commercial PEGylated reagents and the reactive groups in the substrates rather than the optimal properties for the PEGylated targets to be achieved. Therefore, it is of great importance to develop monodisperse PEGylated reagents and study the impact of their monodispersity, geometry, size, and PEGylation sites on the physicochemical and biological properties of the PEGylated targets. The study would not only promote the transformation of PEGylation from an empirical technology to a quantitative science but also significantly benefit related biomedical research in a controllable and precise manner.

To develop PEGylated reagents, a macrocyclic sulfate-based strategy was recently developed in our group.[18−21] Subsequently, M-PEGylation was found to be crucial for quantitatively optimizing physicochemical, pharmacokinetic, and biological properties of M-PEGylated small molecular drugs, peptidic polymers, and imaging agents.[14−16,22−24] Previously, M-PEGylated peptidic polymers were obtained by

Received: October 16, 2019
Revised: December 12, 2019
Published: December 23, 2019

alternatively assembling natural and M-PEGylated amino acids (AAs) into the peptidic backbones, which exhibited interesting self-assembling and thermo-responsive properties (Scheme 1).[25,26] Herein, we M-PEGylated peptidic polymers by introducing side-chain M-PEGylated *L*-lysines and investigated the impact of M-PEGylation strategies, including M-PEG size, PEGylation site, and geometry, on their physicochemical and biological behaviors in the context of our previous results (Scheme 1). Comparing to our previous backbone PEGylation, side-chain PEGylation on l-lysine residues has been extensively used in biopharmaceutical development.[7] In addition, it can not only facilitate the convenient and large scale preparation of M-PEGylated peptidic polymers but also preserve the α-AA-based secondary and higher order structures which are crucial for the biological function of natural and engineered peptidic polymers and proteins. Based on these concerns, 3 octapeptidic polymers ($\mathbf{P_7}$-**8**, $\mathbf{P_{11}}$-**8**, and $\mathbf{P_{23}}$-**8**) and 2 dodecapeptidic polymers ($\mathbf{P_7}$-**12** and $\mathbf{P_{11}}$-**12**) were designed and synthesized from a commercially available *L*-lysine derivative through fluorenylmethyloxycarbonyl (Fmoc)-based solid-phase peptide synthesis (SPPS).

Scheme 1. Previous and Current Strategies on M-PEGylation of Peptidic Polymers

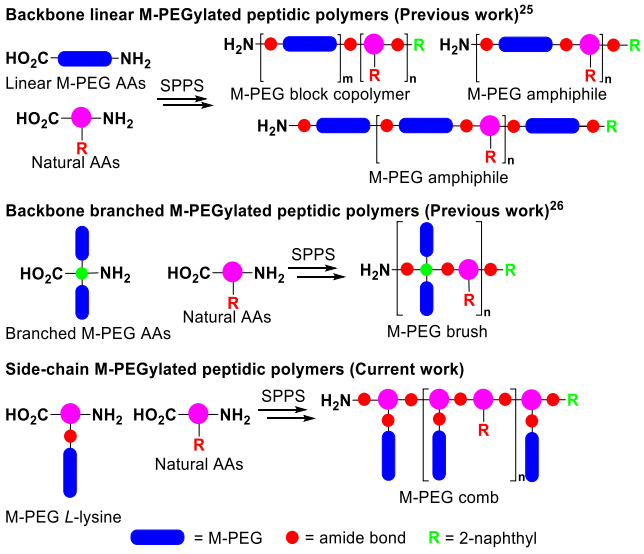

EXPERIMENTAL SECTION

Synthesis and Purification of M-PEGylated Peptidic Polymers. All peptidic polymers were manually synthesized through Fmoc SPPS on Rink amide-AM resin in a sintered glass reaction funnel fitted with a three-way stopcock. After Fmoc-protected AAs (2.5 equiv, relative to the resin loading) and 1-[bis(dimethylamino)-methylene]-1*H*-1,2,3-triazolo[4,5-*b*]pyridinium 3-oxid hexafluoro-phosphate (HATU, 2.4 equiv) or 2-(1*H*-benzotriazole-1-yl)-1,1,3,3-tetrabutylammonium tetrafluoroborate (TBTU, 2.4 equiv) and

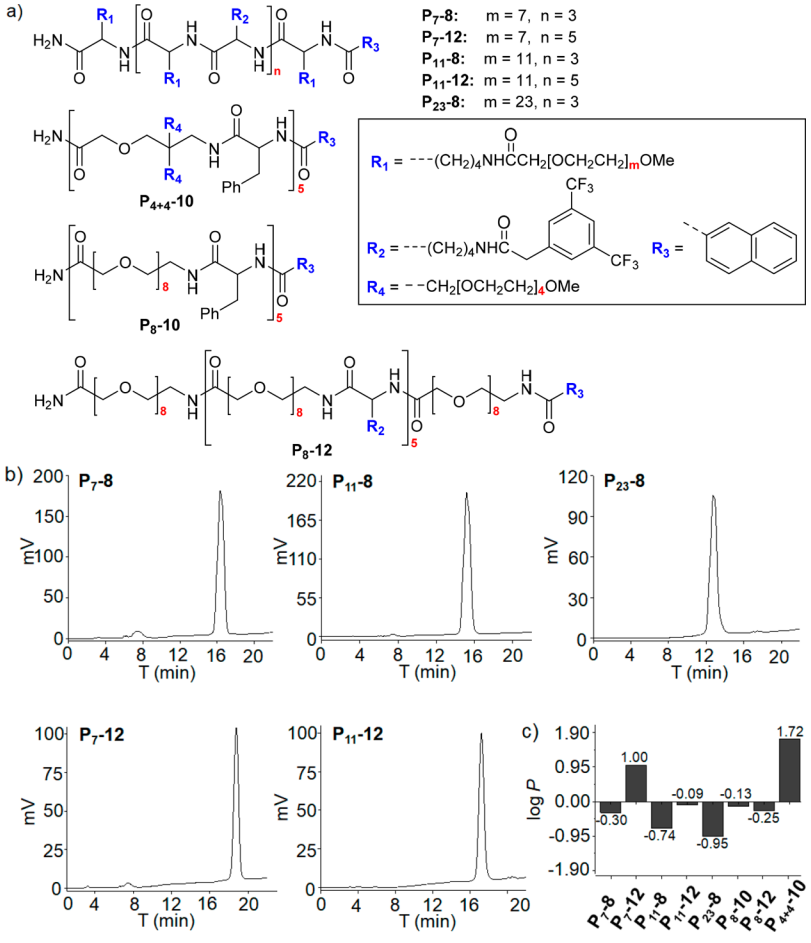

Figure 1. Chemical structure (a), HPLC chromatogram (b), and log *P* of M-PEGylated peptidic polymers (c). HPLC conditions: UV detection at 254 nm, RP C18 column (5 μm; 4.6 × 100 mm), flow rate 0.7 mL/min, and 70% MeOH in water to 100% MeOH over 15 min then 100% MeOH for 5 min.

https://dx.doi.org/10.1021/acs.biomac.9b01425
Biomacromolecules 2020, 21, 725−731

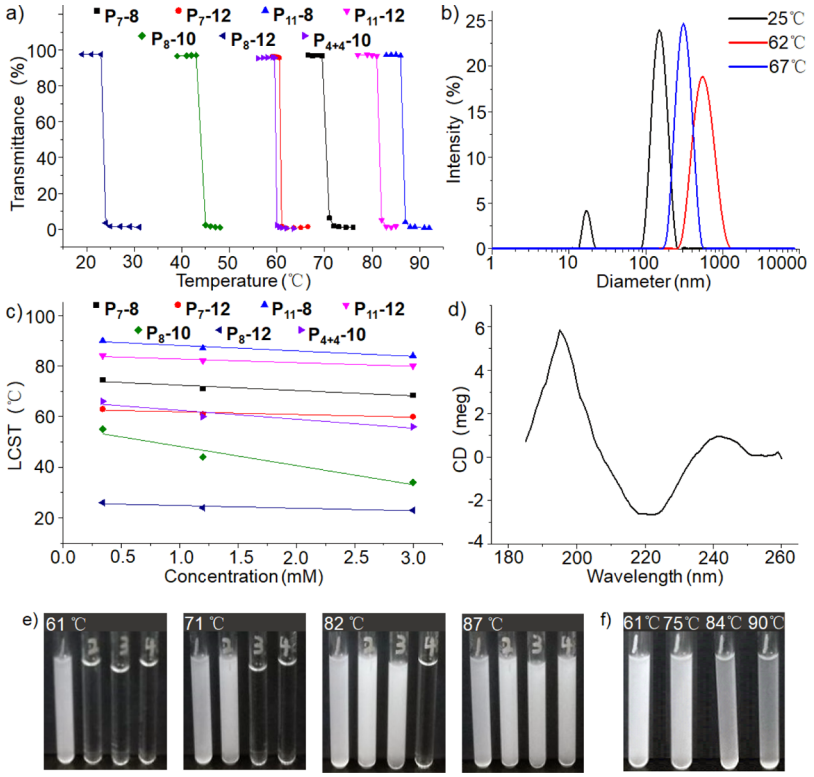

Figure 2. Turbidity curves of M-PEGylated peptidic polymers (a), DLS of $\mathbf{P_7}$-**12** (b), LCST vs concentration of M-PEGylated peptidic polymers (c), CD spectra of $\mathbf{P_7}$-**12** [(d), 0.3 mg/mL, 25 °C], sequential turbidity photos of the M-PEGylated peptidic polymers [(e), tube 1−4 contains 1.2 mM of $\mathbf{P_7}$-**12**, $\mathbf{P_7}$-**8**, $\mathbf{P_{11}}$-**12**, $\mathbf{P_{11}}$-**8**, respectively], and photos (f) of 0.3 mM $\mathbf{P_7}$-**12** at temperatures above its LCST.

hydroxybenzotriazole (HOBt, 2.5 equiv) were dissolved in a minimum amount of dry dimethylformamide (DMF), *N*,*N*-diisopropylethylamine (DIPEA, 5.0 equiv) was added and mixed thoroughly. The solution was added immediately to the resin, and the resulting mixture was agitated with a flow of nitrogen gas under positive pressure for 2−4 h at 25 °C. For each residue, double couplings were carried out. A negative 2,4,6-trinitrobenzenesulfonic acid (TNBS) test was used to confirm the completion of coupling. Once the coupling reaction was completed, the resin was drained under vacuum and washed with dichloromethane (DCM) and DMF several times. Then, the resin was subjected to *N*-Fmoc-protecting group removal by treating the resin with 1,8-diazabicyclo[5.4.0]-undec-7-ene (DBU)/piperidine/DMF (1/1/48 v/v) (8 min, 4 times). Once the desired peptidic polymer sequence was generated, the final Fmoc-protecting group was removed and 2-naphthoic acid was coupled to the *N*-terminal following the coupling procedure. The resin was then thoroughly washed, and the peptidic polymer was cleaved from the resin using trifluoroacetic acid (TFA)/triethylsilane (TES)/DCM (10/1/10 v/v) (40 min, 5 times). All peptidic polymers were purified by preparative reverse phase high-performance liquid chromatography (HPLC, UV detection at 254 nm, RP C18 column (10 μm; 30 mm × 250 mm), gradient elution of 50% methanol in water to 100% methanol over 90 min, flow rate of 10 mL/min).

Preparation of Doxorubicin-Loaded Nanoemulsions. The solvent evaporation method was used for doxorubicin (DOX)-loaded nanoemulsion formulation. DOX·HCl (2 mg) and triethyl amine (TEA) (3 equiv) in 2 mL of DCM were stirred at 25 °C for 3 h. The resulting mixture was evaporated under vacuum. The residue was suspended in 0.2 mL of DCM and combined with a solution of the peptidic polymer (10 mg in 0.2 mL of DCM). The resulting mixture was slowly injected into 5 mL of deionized water under sonicating over 1 h at room temperature. After the organic solvent was evaporated under reduced pressure at room temperature, the DOX-loaded nanoemulsion was obtained by filtering twice through a 0.45 μm polycarbonate membrane.

In Vitro ^{19}F MRI Experiments. Magnetic resonance imaging (MRI) experiments were performed with peptidic polymer $\mathbf{P_7}$-**8** solutions (5.8, 4.4, 3.3, 2.4, and 1.8 mM, prepared by sequential dilution with deionized water) on a 400 MHz Bruker BioSpec MRI system at 25 °C using a gradient-echo (GRE) pulse sequence, rare factor = 4; matrix size = 32 × 32; SI = 37 mm; FOV = 3.7 cm; TR = 3500 ms; TE = 7.0 ms; scan time = 28 s.

Cellular Uptake. $HepG_2$ cells were seeded into confocal dishes and cultured for 24 h. Then, free DOX (5 μg/mL) or the $\mathbf{P_7}$-**12**/DOX nanoemulsion with equivalent DOX was added and the cells were incubated at 37 °C for 0.5 or 2 h, respectively. The supernatant was carefully removed and washed with phosphate-buffered saline (PBS) buffer. After the cells were fixed with 4% formaldehyde for 20 min at room temperature and washed three times with PBS, the cells were stained with 4,6-diamidino-2-phenylindole (DAPI) for 5 min and imaged with confocal laser scanning microscopy (Leica LCS-SP8-STED).

RESULTS AND DISCUSSION

Synthesis and Characterization of M-PEGylated Peptidic Polymers. All side-chain M-PEGylated peptidic polymers were obtained on multihundred milligram scales after HPLC purification (Figure 1). M-PEGylated peptidic "brush" $\mathbf{P_{4+4}}$-**10** and backbone M-PEGylated peptidic polymers $\mathbf{P_8}$-**10** and $\mathbf{P_8}$-**12** from our previous study were employed as comparisons (Figure 1).[25,26] Lipophilicity of the M-PEGylated peptidic polymers was then investigated with reverse-phase HPLC and partition coefficients log *P* (Figure 1). On the one hand, both the HPLC retention time and log *P* showed that the lipophilicity of the lysine side-chain M-PEGylated peptidic polymers decreased with the increase of M-PEG size (log *P*($\mathbf{P_7}$-**8**) > log *P*($\mathbf{P_{11}}$-**8**) > log *P*($\mathbf{P_{23}}$-**8**)) and the decrease of residues (log *P*($\mathbf{P_7}$-**12**) > log *P*($\mathbf{P_7}$-**8**); log *P*($\mathbf{P_{11}}$-**12**) > log *P*($\mathbf{P_{11}}$-**8**)). The same trend was also observed in the backbone

https://dx.doi.org/10.1021/acs.biomac.9b01425
Biomacromolecules 2020, 21, 725−731

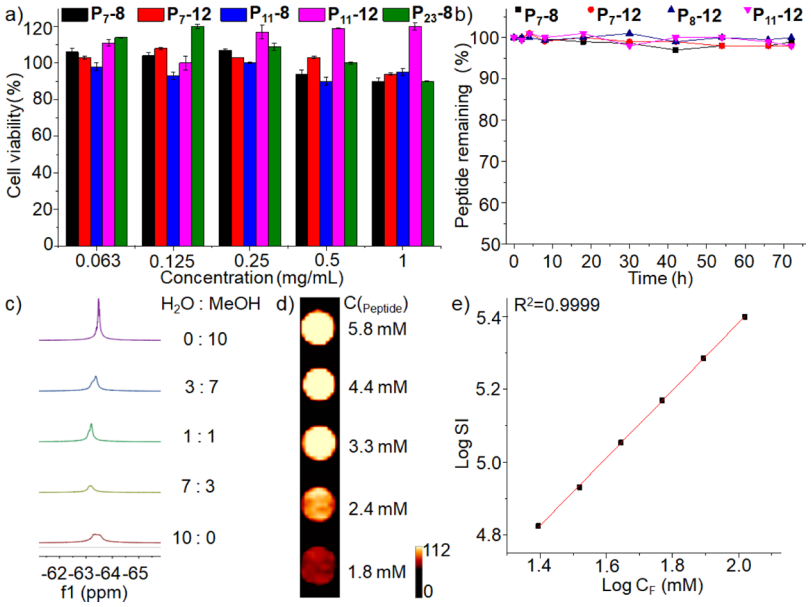

Figure 3. Biocompatibility assay on L929 cells (a) and plasma stability (b) of the side-chain M-PEGylated peptidic polymers, solvent-dependent ^{19}F NMR (c), ^{19}F MRI phantom images (d), and plot of log(SI) vs log $C(^{19}F)$ (e) of peptidic polymer **P_7-8**.

M-PEGylated peptidic polymers. Basically, the lipophilicity of the three types of M-PEGylated peptidic polymers can be fine-tuned by manipulating the size of M-PEG. On the other hand, when replacing the M-PEGylated lysines in peptidic polymer **P_7-12** with M-PEG ω-AAs of similar PEG sizes, the resulting backbone M-PEGylated peptidic polymer **P_8-12** showed dramatically lower lipophilicity. Our previous study showed that, with similar PEG units in the M-PEG AAs, peptidic polymer **P_8-10** with linear M-PEG ω-AAs had far lower lipophilicity than peptidic polymer **P_{4+4}-10** with branched M-PEG AAs.[26] Therefore, when tuning down the lipophilicity of a peptidic polymer by introducing M-PEGylated AAs, the introduction of M-PEG ω-AAs is more efficient than the introduction of the corresponding M-PEGylated lysines and branched M-PEG AAs.

Thermosensitive Behaviors of M-PEGylated Peptidic Polymers. Similar to backbone M-PEGylated peptidic polymers, the side-chain M-PEGylated peptidic polymers showed thermosensitivity with sharp lower critical solution temperatures (LCSTs, Figure 2a,e). It was interesting to find that their thermosensitive properties exhibited many quantitative features. First, it was found that the LCSTs increased with the increase of M-PEG sizes (LCST(**P_7-8**) < LCST(**P_{11}-8**) and LCST(**P_7-12**) < LCST(**P_{11}-12**)) and the decrease of residues (LCST(**P_7-12**) < LCST(**P_7-8**) and LCST(**P_{11}-12**) < LCST(**P_{11}-8**)), which was also observed in the backbone M-PEGylated peptidic polymers. For peptidic polymer **P_{23}-8** with relatively long M-PEGs and less residues, its LCST was too high (>100 °C) to be measured by using the instrument. Second, it was noteworthy that backbone M-PEGylated peptidic polymer **P_8-12** showed dramatically lower LCST, about 37 °C lower, than the corresponding side-chain M-PEGylated peptidic polymer **P_7-12**, while the corresponding backbone-branched M-PEGylated peptidic polymer **P_{4+4}-10** had similar LCSTs as side-chain M-PEGylated peptidic polymer **P_7-12**. These results indicated that not only the PEG and peptidic polymer sizes but also the M-PEG geometry and PEGylation sites had a significant impact on their thermosensitivity. Third, it was found that, for all the M-PEGylated peptidic polymers, their LCSTs were proportional to their concentrations, which facilitated the accurate prediction of an M-PEGylated peptidic polymer's LCST through its LCST-concentration curve (Figure 2c). The functional equations of LCST and concentrations for these M-PEGylated peptidic polymers were calculated, which showed that LCSTs of backbone M-PEGylated peptidic polymer **P_8-10** and branched peptidic polymer **P_{4+4}-10** were much more concentration-dependent than those of side-chain M-PEGylated peptidic polymers. Fourth, when continuously heating the solution of a side-chain M-PEGylated peptidic polymer, the clear solution first became turbid at its LCST and then turned into less turbid above its LCST (Figure 2e,f), which promoted us to study the self-assembly of the peptidic polymers with dynamic light scattering (DLS, Figure 2b). Below LCST, the sizes of peptidic polymer nanoparticles were within 200 nm, which resulted in clear solutions. At a peptidic polymer concentration of 0.9 mg/mL, the particle sizes increased with the increase of total M-PEG in the peptidic polymers, while the polydispersity indexes (PDI) of the nanoparticles remained high (see Table S2). At LCST, the sizes of peptidic polymer nanoparticles expanded to the wavelength of visible light as a result of their thermo-responsive self-assemble behaviors, which resulted in turbid solutions (see Table S3 and Figure S2). Meanwhile, a significant decrease in PDI was also detected in the peptidic polymer solutions at the corresponding LCSTs. When heating the solutions to a temperature slightly above the corresponding LCSTs, decreases in particle sizes and extremely low PDI (as low as 0.042) were detected, which resulted in less turbid solutions (see Table S3 and Figure S2). Therefore, the self-assembly of side-chain M-PEGylated peptidic polymers might have reached highly homogenized thermodynamic equilibrium states at a temperature slightly above LCSTs. It was noteworthy that both backbone linear M-PEGylated peptidic polymer **P_8-12** and branched PEGylated peptidic polymer **P_{4+4}-10** showed similar particle sizes and PDI changes when DLS was employed to study their solutions at a series of temperatures (see Table S3 and Figure S2). Finally, the

https://dx.doi.org/10.1021/acs.biomac.9b01425
Biomacromolecules 2020, 21, 725−731

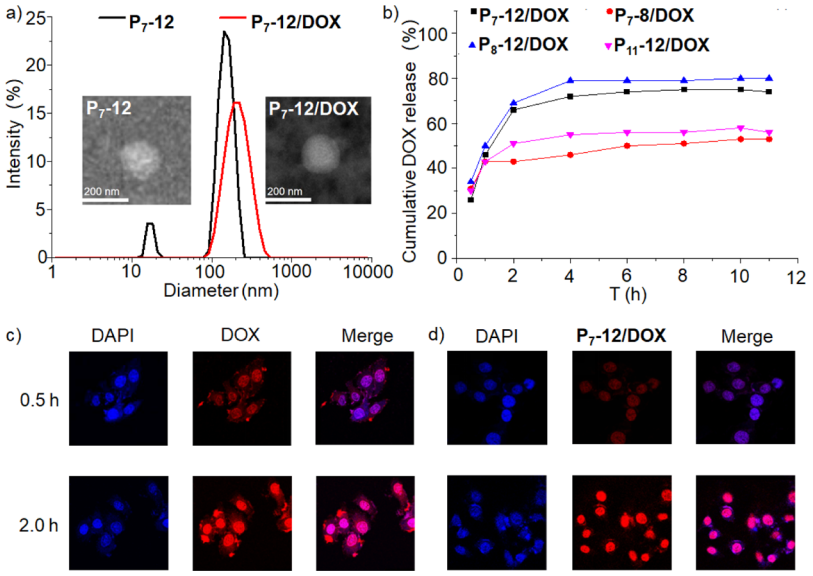

Figure 4. DLS of P_7-**12** and DOX-loaded P_7-**12** with the insertion of transmission electron microscopy (TEM) images (a), DOX release curves of the DOX-loaded peptidic polymer nanoemulsions (b), and confocal images of $HepG_2$ cells treated with DOX and DOX-loaded P_7-**12**, respectively (c,d).

conformation of side-chain M-PEGylated peptidic polymer P_7-**12** was studied with circular dichroism (CD) spectra. A positive peak at 195 nm and a negative peak at 220 nm were found in its CD spectrum (Figure 2d), which indicated that side-chain M-PEGylated peptidic polymer P_7-**12** adopted β-sheet conformations in solution. In contrast, random confirmations were detected for backbone M-PEGylated peptidic polymer P_8-**12**.[25]

Biological Properties of M-PEGylated Peptidic Polymers. The biological and magnetic resonance properties of the M-PEGylated peptidic polymers were then investigated and compared. First, all the side-chain M-PEGylated peptidic polymers (P_7-**8**, P_7-**12**, P_{11}-**8**, P_{11}-**12**, and P_{23}-**8**) showed high biocompatibilities in cytotoxicity assays on murine fibroblast cells (L929 cells, Figure 3a). For the backbone M-PEGylated peptidic polymers, high biocompatibilities were found for linear peptidic polymers with relatively long M-PEGs (P_{12}-**12** and P_{12}-**8**), branched peptidic polymers (P_{4+4}-**10** and P_{12+12}-**10**), and block-copolymer type peptidic polymers, while linear peptidic polymers with relatively short M-PEGs (P_6-**8**, P_8-**8**, and P_8-**12**) showed considerable cytotoxicity toward L929 cells.[25,26] Therefore, the PEGylation site, M-PEG size, and geometry played important roles in the biocompatibility of M-PEGylated peptidic polymers. Second, in vitro stabilities of the M-PEGylated peptidic polymers were evaluated in SD rat plasma. Previously, it was found that backbone-branched M-PEGylated peptidic polymers (P_{4+4}-**10** and P_{12+12}-**10**) showed high plasma stability, while the backbone linear M-PEGylated peptidic polymer (P_8-**10**) exhibited dramatically lower plasma stability. Fortunately, high plasma stabilities were found for all the side-chain M-PEGylated peptidic polymers (Figure 3b), in which the M-PEGs on the lysine side chains may shield the amide bonds from degradation by proteases.

Magnetic Resonance and Fluorescence Properties of M-PEGylated Peptidic Polymers. The multiple fluorines not only promoted the hydrophobic interaction for self-assembly in water but also provided a strong ^{19}F signal for monitoring the peptidic polymers with fluorine-19 magnetic resonance spectroscopy or imaging (^{19}F NMR/MRI) without background signal and ionizing radiation. For peptidic polymer P_7-**8**, a sharp ^{19}F NMR peak from all 18 fluorines was found from its methanol solution and the peak broadened and split when gradually adding water to the solution (Figure 3c), which indicated its hydrophobic interaction-induced self-assembly in water. The multiple fluorines also facilitate the ^{19}F MRI visualization of peptidic polymer P_7-**8** at a low concentration of 1.8 mM with a short scan time of 28 s (Figure 3d). Notably, the ^{19}F MRI signal intensity (SI) of peptidic polymer P_7-**8** is proportional to its ^{19}F concentration, which would be highly valuable for quantitatively tracking the peptidic polymers with ^{19}F MRI (Figure 3e). In addition, the 2-naphthoyl group at the N-terminal provided maximum UV absorption at around 213 nm and maximum fluorescent emission at around 725 nm for monitoring the peptidic polymer with optical methods (see Figure S3).

Drug Delivery Capability of M-PEGylated Peptidic Polymers. As the amphiphilic M-PEGylated peptidic polymers may be promising drug delivery vehicles for ^{19}F MRI and fluorescence dual-imaging-traceable and thermosensitive drug delivery,[25] an in vitro DOX delivery using peptidic polymers (P_7-**8**, P_7-**12**, P_8-**12**, and P_{11}-**12**) was carried out. First, hydrophobic DOX and amphiphilic peptidic polymer P_7-**12** would self-assemble into nanoemulsions with a relatively high drug encapsulation efficiency of 9.0% (the DOX loading capacity of peptidic polymers P_7-**8**, P_7-**12**, P_8-**12**, and P_{11}-**12** were 6.5, 9.0, 6.3, and 7.2%, respectively). After loading DOX, DLS of P_7-**12**/DOX emulsions showed a particle size of 178 nm and a PDI of 0.207, which were comparable to those of P_7-**12** self-assembled particles (176 nm) (Figure 4a). Second, it was important to find that the drug release rate could be tuned by the M-PEGylation site and the M-PEG size (Figure 4b). On the one hand, for the side-chain M-PEGylated peptidic polymers, increasing their residues dramatically speeded up the drug release (P_7-**8** < P_7-**12**), while increasing their M-PEG content significantly slowed down the drug release (P_7-**12** > P_{11}-**12**). On the other hand, side-chain M-PEGylated peptidic polymer P_7-**12** showed slightly slower drug release than that of backbone M-PEGylated peptidic polymer P_8-**12**. Interestingly,

https://dx.doi.org/10.1021/acs.biomac.9b01425
Biomacromolecules 2020, 21, 725−731

the trend of drug release rates in DOX-loaded emulsions was coincident with the log *P* trend of the side-chain M-PEGylated peptidic polymers (log *P*($\mathbf{P}_7$-**12**) > log *P*($\mathbf{P}_{11}$-**12**) > log *P*($\mathbf{P}_7$-**8**)), which suggested that the hydrophobic interactions between DOX and peptidic polymers played a critical role in the drug release rate. Third, confocal microscopy images indicated that DOX can be efficiently delivered into $HepG_2$ cells by loading DOX onto M-PEGylated peptidic polymer $\mathbf{P}_7$-**12** (Figure 4c,d).

CONCLUSIONS

In summary, we have disclosed the impact of PEGylation sites, M-PEG size, and geometry on the lipophilicity, thermosensitivity, biocompatibility, in vitro stability, and drug release profile of M-PEGylated peptidic polymers. Through a comparative physicochemical and biological property study on a series of side-chain and backbone M-PEGylated peptidic polymers, it was found that (1) linear M-PEGylation on the peptidic backbone is more efficient in tuning down the lipophilicity of a peptidic polymer than that on side-chain M-PEGylation and backbone-branched M-PEGylation. (2) M-PEGylated amphiphilic peptidic polymers would exhibit thermosensitivity with sharp LCSTs. Backbone linear M-PEGylated peptidic polymers show dramatically lower LCSTs than the corresponding side-chain M-PEGylated peptidic polymers and backbone-branched M-PEGylated peptidic polymers. It is noteworthy that the LCST of an M-PEGylated peptidic polymer can be accurately predicted from its LCST-concentration curves. (3) For M-PEGylated peptidic polymers, a thermodynamic equilibrium state with highly homogenized peptidic polymer nanoparticles exists above its LCST. (4) Except for the backbone linear M-PEGylated ones, the M-PEGylated peptidic polymers mentioned in this article show high biocompatibility and plasma stability. Besides, the M-PEGylated peptidic polymers exhibit valuable fluorescence and ^{19}F MRI dual-imaging modality. Based on the structure–property relationship study, the M-PEGylated peptidic polymers were employed as drug delivery vehicles and the drug release rate can be fine-tuned by either manipulating the number of residues or the length of M-PEGs in the peptidic polymers. It is necessary to point out that the M-PEGylation strategies developed here enable the quantitative physicochemical and biological study, which laid the solid foundation for the design, synthesis, and optimization of PEGylated peptidic polymers in biomedicine, materials, and beyond.

ASSOCIATED CONTENT

Supporting Information

The Supporting Information is available free of charge at https://pubs.acs.org/doi/10.1021/acs.biomac.9b01425.

Solvent-dependent ^{19}F NMR, log *P*, turbidity test, DLS, TEM, IC_{50} and cytotoxicity assay, cell uptake, UV and fluorescent property, stability study in rat plasma, and copies of spectra (PDF)

AUTHOR INFORMATION

Corresponding Authors

Xin Zhou − *Chinese Academy of Sciences, Wuhan, China;* orcid.org/0000-0002-5580-7907; Email: xinzhou@wipm.ac.cn

Zhong-Xing Jiang − *Wuhan University, Wuhan, China;* orcid.org/0000-0003-2601-4366; Email: zxjiang@whu.edu.cn

Other Authors

Xuemeng Wang − *Wuhan University, Wuhan, China*

Yu Li − *Chinese Academy of Sciences, Wuhan, China*

Tingjuan Wu − *University of South China, Hengyang, China*

Zhigang Yang − *Wuhan University, Wuhan, China;* orcid.org/0000-0002-4857-4850

Xing Zheng − *University of South China, Hengyang, China*

Shizhen Chen − *Chinese Academy of Sciences, Wuhan, China*

Complete contact information is available at: https://pubs.acs.org/10.1021/acs.biomac.9b01425

Notes

The authors declare no competing financial interest.

ACKNOWLEDGMENTS

We are thankful for financial support from the National Key R&D Program of China (2016YFC1304704 and 2018YFA0704000), the National Natural Science Foundation of China (21572168 and 81625011), and the Key Research Program of Frontier Sciences, CAS (QYZDY-SSW-SLH018).

REFERENCES

(1) Harris, J. M.; Chess, R. B. Effect of PEGylation on pharmaceuticals. *Nat. Rev. Drug Discovery* **2003**, *2*, 214−221.

(2) Knop, K.; Hoogenboom, R.; Fischer, D.; Schubert, U. S. Poly(ethylene glycol) in drug delivery: pros and cons as well as potential alternatives. *Angew. Chem., Int. Ed.* **2010**, *49*, 6288−6308.

(3) Parrott, M. C.; DeSimone, J. M. Relieving PEGylation. *Nat. Chem.* **2012**, *4*, 13−14.

(4) Herzberger, J.; Niederer, K.; Pohlit, H.; Seiwert, J.; Worm, M.; Wurm, F. R.; Frey, H. Polymerization of ethylene oxide, propylene oxide, and other alkylene oxides: synthesis, novel polymer architectures, and bioconjugation. *Chem. Rev.* **2016**, *116*, 2170−2243.

(5) Cui, J.; Björnmalm, M.; Ju, Y.; Caruso, F. Nanoengineering of poly(ethylene glycol) particles for stealth and targeting. *Langmuir* **2018**, *34*, 10817−10827.

(6) Veronese, F. M.; Pasut, G. PEGylation, successful approach to drug delivery. *Drug Discovery Today* **2005**, *10*, 1451−1458.

(7) Veronese, F. M.; Mero, A. The impact of PEGylation on biological therapies. *BioDrugs* **2008**, *22*, 315−329.

(8) Fishburn, C. S.; Pharm, J. The pharmacology of PEGylation: balancing PD with PK to generate novel therapeutics. *J. Pharm. Sci.* **2008**, *97*, 4167−4183.

(9) Suk, J. S.; Xu, Q.; Kim, N.; Hanes, J.; Ensign, L. M. PEGylation as a strategy for improving nanoparticle-based drug and gene delivery. *Adv. Drug Delivery Rev.* **2016**, *99*, 28−51.

(10) Chapman, A. P.; Antoniw, P.; Spitali, M.; West, S.; Stephens, S.; King, D. J. Therapeutic antibody fragments with prolonged in vivo half-lives. *Nat. Biotechnol.* **1999**, *17*, 780−783.

(11) Seely, J. E.; Richey, C. W. Use of ion-exchange chromatography and hydrophobic interaction chromatography in the preparation and recovery of polyethylene glycol-linked proteins. *J. Chromatogr. A* **2001**, *908*, 235−241.

(12) Haag, R.; Kratz, F. Polymer therapeutics: concepts and applications. *Angew. Chem., Int. Ed.* **2006**, *45*, 1198−1215.

(13) Vicent, M. J.; Dieudonné, L.; Carbajo, R. J.; Pineda-Lucena, A. Polymer conjugates as therapeutics: future trends, challenges and opportunities. *Expert Opin. Drug Delivery* **2008**, *5*, 593−614.

(14) Yu, Z.; Bo, S.; Wang, H.; Li, Y.; Yang, Z.; Huang, Y.; Jiang, Z.-X. Application of monodisperse PEGs in pharmaceutics: monodisperse polidocanols. *Mol. Pharm.* **2017**, *14*, 3473−3479.
(15) Deng, T.; Mao, X.; Li, Y.; Bo, S.; Yang, Z.; Jiang, Z.-X. Monodisperse oligoethylene glycols modified Propofol prodrugs. *Bioorg. Med. Chem. Lett.* **2018**, *28*, 3502−3505.
(16) Deng, T.; Mao, X.; Xiao, Y.; Yang, Z.; Zheng, X.; Jiang, Z.-X. Monodisperse oligoethylene glycols modified camptothecin, 10-hydroxycamptothecin and SN38 prodrugs. *Bioorg. Med. Chem. Lett.* **2019**, *29*, 581−584.
(17) Leroux, J.-C. Editorial: Drug Delivery: Too Much Complexity, Not Enough Reproducibility? *Angew. Chem., Int. Ed.* **2017**, *56*, 15170−15171.
(18) Zhang, H.; Li, X.; Shi, Q.; Li, Y.; Xia, G.; Chen, L.; Yang, Z.; Jiang, Z.-X. Highly efficient synthesis of monodisperse poly(ethylene glycols) and derivatives through macrocyclization of oligo(ethylene glycols). *Angew. Chem., Int. Ed.* **2015**, *54*, 3763−3767.
(19) Xia, G.; Li, Y.; Yang, Z.; Jiang, Z.-X. Development of a scalable process for α-amino-ω-methoxyl-dodecaethylene glycol. *Org. Process Res. Dev.* **2015**, *19*, 1769−1773.
(20) Wan, Z.; Li, Y.; Bo, S.; Gao, M.; Wang, X.; Zeng, K.; Tao, X.; Li, X.; Yang, Z.; Jiang, Z.-X. Amide bond-containing monodisperse polyethylene glycols beyond 10,000 Da. *Org. Biomol. Chem.* **2016**, *14*, 7912−7919.
(21) Lv, X.; Zheng, X.; Yang, Z.; Jiang, Z.; Jiang, Z.-X. One-pot synthesis of monodisperse dual-functionalized polyethylene glycols through macrocyclic sulfates. *Org. Biomol. Chem.* **2018**, *16*, 8537−8545.
(22) Bo, S.; Song, C.; Li, Y.; Yu, W.; Chen, S.; Zhou, X.; Yang, Z.; Zheng, X.; Jiang, Z.-X. Design and synthesis of fluorinated amphiphile as ^{19}F MRI/fluorescence dual-imaging agent by tuning the self-assembly. *J. Org. Chem.* **2015**, *80*, 6360−6366.
(23) Liu, X.; Yuan, Y.; Bo, S.; Li, Y.; Yang, Z.; Zhou, X.; Chen, S.; Jiang, Z.; Jiang, Z.-X. Monitoring fluorinated dendrimer-based self-assembled drug-delivery systems with ^{19}F magnetic resonance. *Eur. J. Org. Chem.* **2017**, 4461−4468.
(24) Bo, S.; Yuan, Y.; Chen, Y.; Yang, Z.; Chen, S.; Zhou, X.; Jiang, Z.; Jiang, Z.-X. In vivo drug tracking with ^{19}F MRI at therapeutic dose. *Chem. Commun.* **2018**, *54*, 3875−3878.
(25) Zhu, J.; Xiao, Y.; Zhang, H.; Li, Y.; Yuan, Y.; Yang, Z.; Chen, S.; Zheng, X.; Zhou, X.; Jiang, Z.-X. Peptidic monodisperse PEG "combs" with fine-tunable LCST and multiple imaging modalities. *Biomacromolecules* **2019**, *20*, 1281−1287.
(26) Li, Y.; Wang, X.; Chen, Y.; Yang, Z.; Jiang, Z.-X. Monodisperse polyethylene glycol "brushes" with enhanced lipophilicity, and thermo and plasma stability. *Chem. Commun.* **2019**, *55*, 1895−1898.

https://dx.doi.org/10.1021/acs.biomac.9b01425
Biomacromolecules 2020, 21, 725−731